Scattering of atomic matter waves from ridged surfaces

Dmitrii Kouznetsov* and Hilmar Oberst

Institute for Laser Sciences, University of Electro-Communications, 1-5-1 Chofugaoka, Chofu-shi, Tokyo 182-8585, Japan

Motivated by recent experiments that demonstrated a strongly enhanced reflection efficiency of atoms on microfabricated, gratinglike surface structures, we develop a detailed description of the scattering of atomic matter waves on such structures. We start with a simple model that describes the ridged surface as an equivalent absorbing medium. This model correctly predicts the experimentally observed scaling and magnitude of the reflection efficiency. We then calculate the accurate solutions for the Fresnel diffraction of waves at grazing incidence at a periodic set of idealized, parallel edges. Both numerical and analytical solutions are presented. The specular reflectivity and its phase, as well as the efficiencies of higher diffraction orders are calculated. We compare our results to experimental data in a wide range of parameters. We extend the model including the finite size of the grating ridges and the van der Waals attraction and suggest a more general estimate of the reflection coefficient.

PACS number(s): 03.75.Be, 03.65.Xp, 34.50.Dy

I. INTRODUCTION

Atom optics is a very active field of physics. The performance of atom optical devices improves from year to year. Microfabricated surface structures to trap and channel atoms (atom chips) were developed [1,2]. Nanoscale structures with extremely narrow localization of light fields (photon dots and holes) allow the manipulation of cold atoms on a submicron scale [3]. Atomic mirrors are also important elements necessary in atomic optics. Such mirrors may use an evanescent optical wave [4–6] or magnetic fields [7–9]. These mirrors reflect nearly all of the incident atoms with an artificially created repulsive potential; however, it is quite difficult to make these mirrors large without compromising their accuracy.

Attempts to make efficient solid-state atomic mirrors can be traced back to the last century. Unfortunately, the efficiency of the reflection of atoms at room temperature is not high even at grazing incidence. The repulsion of atoms from surfaces occurs at small distance of order of atomic size; therefore, such a reflection is mainly incoherent (see Refs. [10,11] and references therein). The coherence of the reflection improves as atoms become slower. The reflection of atoms by surfaces can occur when the de Broglie wavelengths corresponding to the atomic motion perpendicular to the interface is larger than the characteristic length associated with the surface [12]. Serious improvement of the reflectivity of solid-state atomic mirrors was achieved with cold atomic matter waves [13]. The long-range attraction near a solid surface is the van der Waals interaction; it can be approximated by the potential $U(y) = -C_4/[(y+\rho_0)y^3]$ as a function of the coordinate y orthogonal to the plane of the mirror. Classically, we would expect the atom to accelerate toward the surface and ultimately scatter or be adsorbed. However, when the atom is sufficiently slow, the wave nature of the atoms leads to the reflection of the incident wave at a steep

slope of the potential. Such reflections have been called "quantum reflections" [12–21]. This phenomenon has previously been known to occur when cold atoms are incident on liquid He surfaces [22–25]. Following the first experiment that measured the reflectivity of laser-cooled metastable neon atoms (Ne*) on silicon and glass surfaces [26], the quantum reflection on solid surfaces has been studied using different atomic species and surface materials [27,28].

The main problem with coherent atom mirrors based on solid surfaces is that the reflection coefficient decreases quickly with increasing transversal wave number $k_y = Mv/\hbar$, where M is the mass of the atom and v is the normal component of its velocity. In most cases, the atom mirrors work at small values of the grazing angle $\theta = \arcsin(v/V)$, where V is velocity of the atom. This low reflectivity still strongly limits the applicability of solid surfaces as atom reflectors. In order to improve the efficiency of the specular reflection, either the potential constant C_4 or the normal component v of the velocity should be reduced. Recently, a significant improvement of the reflectivity was achieved by using microfabricated surface structures, consisting of narrow parallel ridges [26,29–31] such as shown in Fig. 1(a). The idea was to reduce the effective van der Waals constant by reducing the effective density of the material; the corresponding effective van der Waals constant [29] was expected to be of order
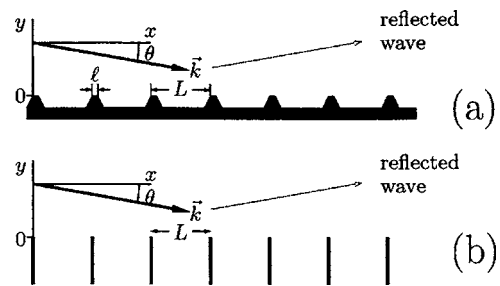

FIG. 1. (a) Wave with wave vector $\vec{k}$ incident at the grazing angle θ onto the surface with a grating structure. (b) The idealization of the structure as a periodical set of absorbers.

---

*Electronic address: dima@ils.uec.ac.jp

of $(\ell/L)C_4$, where L is the distance between ridges and ℓ is their width [Fig. 1(a)]. However, this scaling of the constant overestimates the reflectivity and shows only qualitative agreement with experiments. The reduction of the distance L at fixed values of ℓ and k leads to an increase of the effective potential; this could lead to the reduction of the reflectivity. Actually, the reflectivity increases as we reduce L. For the development of efficient atomic mirror, a quantitative description of the phenomenon is required. We suggest such a description here.

Experiments performed in our institute have revealed that the reflection coefficient on the ridged surface structures depends mainly on the dimensionless parameter $p=\sqrt{kL}\theta$ [31,32], where $k=MV/\hbar$ is the wave number. This property could be explained by assuming that the reflection is caused by the Fresnel diffraction at an array of ridges. In the previous papers, only a qualitative derivation was presented, and the accurate solution was mentioned without proof.

In this paper, we present various derivations of the reflection and diffraction efficiencies of atomic matter waves incident at small grazing angle on an array of idealized thin ridges. Then we analyze the effect of finite width of the ridges. We take into account the van der Waals potential and compare the results with experimental data in wide range of parameter values (Table I).

We do not need any particular assumption about the state of the atoms. Therefore, our estimates can be applied to both atoms in the ground state and to atoms in the excited states. Ground state atoms are interesting from the point of view of atom microscopy. The low energy of atoms makes the probing process nondestructive [10]. The use of excited atoms allows their efficient detection with high resolution using semiconductor detectors [13,26,31]. The ridged mirror designed for the excited atoms will work as well for the ground-state atoms. This is the justification for working with excited atoms.

The paper is organized as follows: We start in Sec. II with the derivation of a simple estimate that is obtained by assuming that the ridged surface behaves like an equivalent medium with effective absorption rate V/L. Such an approach leads to the same equations and estimates, as the interpretation of ridged surface as detectors and the following interpretation of the reflection in terms of the the Zeno effect [32]. In Sec. III, we describe the numerical simulation of the diffraction process using the beam propagation method [33–36]. In Sec. IV, we apply the formalism of coupled waves and cross-reflection coefficients [37–40]. Then, in Sec. V, we suggest a correction to our estimate that takes into account the finite width of the ridges and the van der Waals potential near the ridges.
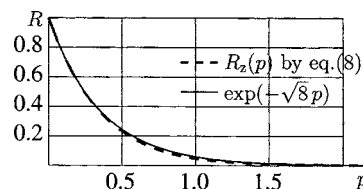

FIG. 2. Function $R_z(p)$ by Eq. (8) (dashed line) and the fit $\exp(-\sqrt{8}p)$ (solid line).

II. SIMPLE ESTIMATE

In the experiments we want to describe with our model, the surface consisted of a grating structure with period L with parallel ridges that had a width at the top ℓ, as shown in Fig. 1(a). The atoms are incident at small grazing angle θ onto the structure. While $L \gg \ell$, we idealize the surface structure as a periodic set of very thin edges that completely block the incident wave in the lower half-plane ($y < 0$) as is shown in Fig. 1(b).

As a first step, we simplify the description even further by assuming that the set of ridges behaves like an equivalent continuous medium with absorption rate V/L, where V is the velocity of atoms. This assumption leads to the estimate R_z of the reflection coefficient (Fig. 2) obtained in [32] from speculations about the Zeno effect. Below we suggest an alternative way.

A. Equations

Let Ψ be the part of the scattering wave function which represents the atom that has not yet interacted with the surface. Ψ must satisfy the equation

$$[\nabla^2 + k^2 + i\gamma^2 \vartheta(y)]\Psi = 0, \tag{1}$$

where $k=MV/\hbar$ is the wave number, M is the mass of the atom, V is the velocity, ϑ is the Heaviside step function, and γ is the parameter that describes the absorption by the equivalent medium. Following our interpretation of the ridged surfaces as continuously absorbing medium, we set $\gamma^2=k/L$. Considering the two-dimensional case, we construct the solution in the form

$$\Psi = \begin{cases} e^{ik_x x + ik_y y} - re^{ik_x x - ik_y y}, & y \geqslant 0, \\ (1-r)e^{ik_x x + (i\alpha - \beta)y}, & y \leqslant 0, \end{cases} \tag{2}$$

where $k_x=k\cos\theta$, $k_y=-k\sin\theta$. Outside the absorber the wave consists of the incoming and reflected part; inside the absorber the wave is exponentially decaying. Substitution of (2) into (1) gives the equations for the parameters α and β,

$$\alpha^2 - \beta^2 = k_y^2, \tag{3}$$

TABLE I. Physical parameters of experiments with cold atoms.

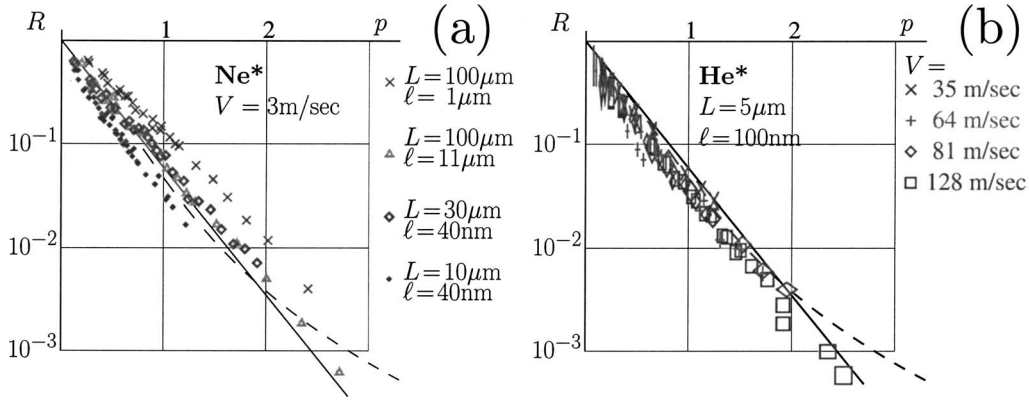| Unit	M amu	C_4 10^{-56} J m^4	v cm/s	V m/s	$\lambda=2\pi/k$ nm	ℓ nm	L μm	Reference
Ne*	20	12	From 2 to 37	3	7	From 40 to 11000	From 10 to 100	[29]
He*	4	8	From 3 to 154	From 35 to 128	From 0.8 to 4	100	5	[31]

FIG. 3. Comparison of the estimate R_z (dashed curve) by Eq. (8) to the experimental data. (a) Reflectivity of Ne* with velocity V =3 m/s from various microfabricated ridged Si surface structures [29]. (b) Similar data for He* atoms reflected on a sample with L =5 μm and ℓ=100 nm with various incident velocities [31].

$$2\alpha\beta = \gamma^2. \tag{4}$$

The appropriate solution is

$$\alpha = \sqrt{\tfrac{1}{2}(\sqrt{k_y^4 + \gamma^4} + k_y^2)}, \tag{5}$$

$$\beta = \sqrt{\tfrac{1}{2}(\sqrt{k_y^4 + \gamma^4} - k_y^2)}. \tag{6}$$

An equation for the complex reflection amplitude r is readily obtained using the continuity of the derivative of $\Psi(x,y)$ at $y=0$,

$$r = \frac{i\alpha - \beta + ik_y}{i\alpha - \beta - ik_y}. \tag{7}$$

We interpret the ratio k_y/k_x as $\tan(\theta)$, see Fig. 1. For the small values of grazing angle θ, we write $k_y/k_x = \theta$. Then, after some algebra, we express the reflection coefficient rr^* in the following form:

$$rr^* = R_z(p) = \frac{\sqrt{\sqrt{1/p^4 + 1} + 1} - \sqrt{2}}{\sqrt{\sqrt{1/p^4 + 1} + 1} + \sqrt{2}}, \tag{8}$$

where

$$p = \sqrt{kL}\,\theta = \sqrt{\frac{ML}{\hbar V}}\,\theta \tag{9}$$

has the meaning of a dimensionless transversal wave number, or dimensionless transversal momentum. This parameter is proportional to parameter $\beta = \sqrt{(\pi/2)}p$ used in our previous paper [31].

The function $R_z(p)$ by (8) can be approximated by the exponential fit $\exp(-\sqrt{8}p)$; the absolute difference between these two functions does not exceed 2%. Both curves are shown in Fig. 2. The reflectivity calculated in Eq. (8) depends only on the parameter p, which demonstrates the scaling law for the reflectivity of waves on a ridged surface.

B. Comparison with experimental data

In this section, we compare our estimate (8) and the exponential fit $\exp(-\sqrt{8}p)$ to various experimental data for the reflection of cold atoms from ridged silicon surfaces. We collect the data from Ref. [29] measured with metastable neon (Ne*) atoms in the $1s_3$ state, and from Ref. [31] measured with metastable helium atoms (He*) in the $2\,^3S_1$ state. In these experiments the atomic beams have been prepared by releasing laser-cooled atoms from magneto-optical traps. The metastable atoms have a high internal energy, 16.6 eV for Ne* and 19.8 eV for He*. They are quenched with high probability upon collision with the short-range core potential. Only specularly reflected metastable atoms have been detected in the experiment. This detection allowed to measure the reflectivity.

In Fig. 3 we compare the reflectivity measured on various samples versus the dimensionless parameter p defined by Eq. (9). The dashed curve represents the estimate (8), and the solid line shows the fit $R = \exp(-\sqrt{8}p)$. (We use the logarithmic scale.) Our estimate explains the almost exponential decay of the reflection coefficient as a function of the grazing angle, as was observed in the experiments. In addition, it also predicts the correct slope of this decay. Equation (8) shows good agreement with the data for Ne* and He* atoms for a wide range of parameter values; these parameters are summarized in Table I.

Considering the strong simplifications of this model, the good agreement with experimental data is quite surprising. The assumption of a continuous absorbing medium ignores the periodical character of the absorbers, so it cannot be used for the analysis of higher orders of scattering. Similarly, it cannot predict the effect of the finite width ℓ of the ridges and that of the van der Waals interaction near the ridges.

As we will see in the following sections, the diffraction at an idealized set of edges leads to a reflectivity that is higher than the measured values. On the other hand, the van der Waals potential near a ridge of finite width is expected to reduce the reflectivity. It happened that several effects partially compensate each other so that our simple estimate agrees quite well, at least in the experimentally investigated parameter range (Table I). In order to reveal the role of each of these effects, we should analyze more carefully the case with discrete idealized ridges.

III. NUMERICAL SIMULATIONS

The estimate (8) provides an unexpectedly good description of experiments that study the reflection of various cold atoms from various ridged Si surfaces [29,31]. Such an approach does not take into account the periodicity of the structure and cannot predict the efficiency of various orders of scattering. In this section, we apply the beam propagation method [33–35] to obtain a numerical solution of the diffraction process; the ridges are treated as ideal, absorbing half-planes [Fig. 1(b)].

A. Equations

The free-space equation

$$\nabla^2 \psi + k^2 \Psi = 0 \tag{10}$$

can be used for the propagation of monochromatic atomic waves between the ridges. As the problem is two-dimensional, we consider a function of only two coordinates. According to Fig. 1, the initial wave vector has the components $k_x = k \cos(\theta) \approx k - k\theta^2/2$, $k_y = -k \sin(\theta) \approx -k\theta$. The incident field Ψ_{in} can be written as follows:

$$\Psi_{in}(x,y) = \exp(ik_x x + ik_y y). \tag{11}$$

In the typical case, the grazing angle θ between the beam and the ridged surface is small, i.e., only several milliradians. Therefore, the paraxial approximation is suitable. We construct the approximate solution of Eq. (1) in the following form:

$$\Psi = \psi(x,y)e^{ikx}. \tag{12}$$

The substitution of Eq. (12) into Eq. (10) and neglecting the term with second x-derivative leads to the well-known equation of Ginsburg-Landau,

$$2ik\frac{\partial}{\partial x}\psi + \frac{\partial^2}{\partial y^2}\psi = 0. \tag{13}$$

The incident field corresponds to

$$\psi_{in} = \exp(-ikx\theta^2/2 - ik\theta y). \tag{14}$$

The distance L between the ridges is used as the unit of length along the x axis. We define the dimensionless coordinates $X = x/L$ and $Y = y\sqrt{k/L}$. Let $\psi(x,y) = E(X,Y)$. Then the incident wave can be written as follows:

$$E_{in}(X,Y) = e^{-ipY - i(p^2/2)X}, \tag{15}$$

where $p = \sqrt{kL}\theta$, and Eq. (13) takes the form

$$2i\frac{\partial}{\partial X}E + \frac{\partial^2}{\partial Y^2}E = 0. \tag{16}$$

In order to represent the ideally absorbing ridge, at integer values of X, we replace $E(X,Y)$ with 0 for all negative values of Y. This replacement, together with Eq. (16) defines our approximation.

B. Numerical algorithm

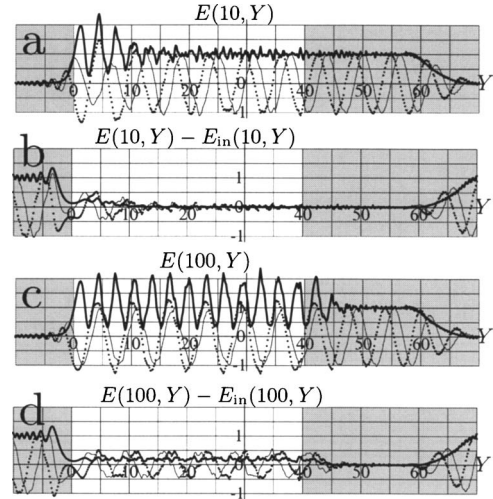For the numerical implementation of the dimensionless equation (16), we use the beam-propagation method [34–36].

FIG. 4. (a) Field E at the initial stage of simulation, $p=1$, $X=10$, $N=1024$, intensity (thick curve), real (thin curve), and imaginary (dotted curve) parts; just before being cut by the absorbing ridge. (b) The same representation for $E - E_{in}$. (c),(d) The same at the final stage of simulation, $X=100$.

Examples of the resulting complex field are shown in Fig. 4. These fields were calculated in the following way. For the propagation of the field, we use

$$E(X,Y) = \frac{1}{\sqrt{2\pi}}\int_{-\infty}^{\infty} e^{-iqY - i(q^2/2)X} F(q)dq. \tag{17}$$

The Fourier representation of the incident wave can be expressed in terms of the δ-function,

$$F_{in}(q) = \sqrt{2\pi}\delta(p+q). \tag{18}$$

For the grid representation, we numerate the grid point with n, $0 \leq n < N$. We take a step of the grid $d = \sqrt{2\pi/N}$,

$$E(X,(n-N/2)d) \rightarrow E_n(X), \tag{19}$$

$$F((n-N/2)d) \rightarrow F_n. \tag{20}$$

Then we replace the integral in Eq. (17) with the sum

$$\frac{1}{\sqrt{2\pi}}\int_{-\infty}^{\infty}\cdots dq \rightarrow \frac{1}{\sqrt{N}}\sum_{n=0}^{N-1}\cdots \tag{21}$$

and get the discrete representation for the integral (17).

We search for the solution of Eq. (16) as the sum of E_{in} and a field propagating to a direction somewhere between the x and y axes, at least in the half-space $y > 0$. In order to work with relatively compact grids, the special source of the incident wave is placed at the top of the computational domain shown with shadowed region on the right-hand side of Fig. 4. Such a source of the incident field is analogous to the approximate image used in Refs. [34,35]; it allows to keep the desirable properties of the field in the vicinity of the boundary of the computational domain. The source of the incident wave has smooth edges, so it absorbs the scattered waves isolating the right-hand boundary of the domain from the left-hand boundary. Therefore, the width of the grid has
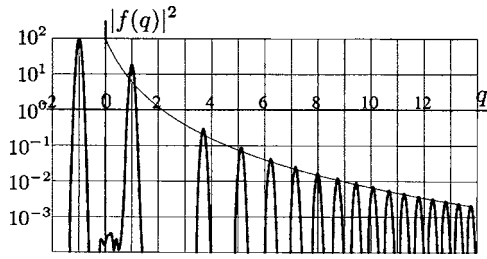
FIG. 5. Intensity of the Fourier transform of the central part of the field evaluated by expression (22) for width $W=10$, $Y_0=30$, $X=800$, $N=4096$ (thick curves); fit (29) scaled with coefficient W^2 (thin curve).

no need to be an integer factor of $2\pi/p$. Such a scheme allows the numerical integration of the Eq. (16) with step equal to unity (i.e., distance between ridges).

In Fig. 4 we show calculation for $p=1$ at a grid of $N=1024$ points. Distributions of field at $X=10$ and $X=100$ are plotted. The left shadowed region indicates the part of the grid which represents the absorbing ridges. The right shadowed region is used to generate the incident field. Initially ($X=0$), all the computational domain is filled with the incident wave. This wave propagated toward the ridges and scatters there. The scattered waves go right, back to the source of incident wave; this source absorbs them. At $X=10$, the scattered waves have not yet propagated far, but at $X=100$ they fill the central part of the computational domain. The fringes appear mainly due to the specular reflection. The region around the center of the domain is used for the analysis of the scattered waves.

C. Analysis of the scattering efficiency

For the spectral analysis of the scattered waves, the region of width W around the center of the grid was used. The field was multiplied by a Gaussian of width W, i.e., $\exp[-(Y-Y_0)^2/2W^2]$ and the Fourier transform

$$f(q) = \frac{1}{\sqrt{2\pi}} \int e^{-iqY} E(X,Y)\exp\left(-\frac{(Y-Y_0)^2}{2W^2}\right)dY \quad (22)$$

was calculated. An example of the resulting momentum distribution of the scattered wave for $p=1$ is shown in Fig. 5. As expected for a grating structure, the momentum distribution shows a discrete spectrum of diffraction orders. Each component appears as a Gaussian of width $1/W$. Their positions q_m are determined by the phase-matching condition

$$q_m = \sqrt{p^2 + 4\pi m}, \quad (23)$$

where the integer m enumerates the orders of scattering. However, the negative mth order will be a wave propagating away from the surface, only if q_m is positive. In this case, the ratio

$$R_m = |f(q_m)|^2/W^2 \quad (24)$$

evaluates the intensity of the mth diffraction order. In experiments with cold atoms, we measure the total number of scattered atoms, which is proportional to the scattering angle. In

order to compare our calculation to experimental results, we should therefore define the scattering efficiency as follows:

$$S_m(p) = \frac{q_m(p)}{p} R_m(p). \quad (25)$$

We calculate and analyze the scattered field for various incident angles, and obtain the scattering efficiencies as a function of the normalized momentum p. This result is shown in Fig. 6, for the specular reflection and the plus or minus first and plus or minus second diffraction orders. The minus first order appears at $p=\sqrt{4\pi}$, the minus second order appears at $p=\sqrt{2\times 4\pi}$, and so on. The intensities of positive orders of scattering ($m>0$) are small compared to that of the specular reflection ($m=0$). At the same time, the negative orders ($m<0$) are much stronger. This gives hope to observe them in experiments with cold atoms. The orders m of scattering are indicated with digits; the characters A and B show the minus first and minus second orders. The circles show the total efficiency $\tilde{s}_8$ of scattering into orders $m<9$, i.e.,

$$\tilde{s}_8(p) = \sum_{m<9} S_m(p). \quad (26)$$

Practically, this total scattering efficiency is determined by the efficiency of scattering into the two lowest orders; the increase of the number of terms in the sum should not change much the estimate of the total scattering efficiency, $\tilde{s}_\infty(p) \approx \tilde{s}_8(p)$. At $p<3$, most of scattering goes to the specular reflection, which validates one of the assumptions used in the analytical estimate of the reflectivity in Refs. [31,32]; there, we had neglected all the scattering waves with $m\neq 0$.

In the case of specular reflection, $m=0$, and we have $S_0(p)=R_0(p)$. For $p<3.6$, this function can be fitted as

$$S_0(p) = R_0(p) \approx \exp[-1.68(1+0.018p^2)p \pm 2\%]. \quad (27)$$

In the same range, a similar expression also fits the total scattering efficiency (25),

$$\tilde{s}_\infty(p) \approx \tilde{s}_8(p) \approx \exp[-1.547(1+0.01p^2)p \pm 2\%]. \quad (28)$$

These fits are shown in Fig. 6 as thin solid lines; they practically coincide with the simulated data (circles) at $p<3.6$.
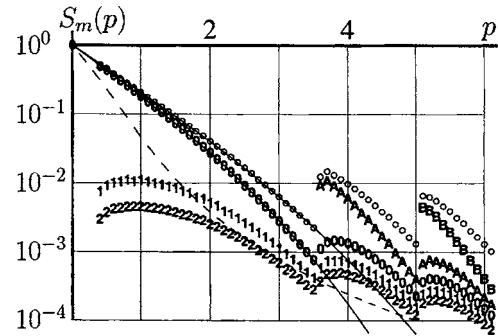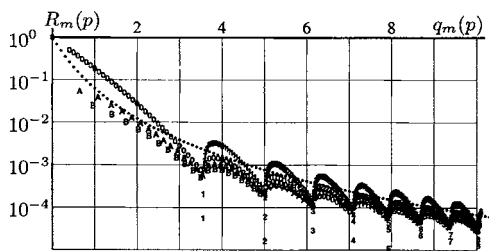

FIG. 6. Efficiency $S_m(p)$ of scattering of particular orders by Eq. (25) (digits) and $\tilde{s}_8(p)$ by (29) (circles) calculated from the simulations; $R(p)$ by (8), dashed; fits (27) and (28), solid.

FIG. 7. Reflectivity $R_m(p)$ of various orders of scattering versus scattering angle $q_m(p)$, digits; estimate by (29), dotted.

The reflectivities R_m by Eq. (24) approximately follow a smooth trend:

$$R_m \approx \frac{1}{(1 + q_m)^4} = \frac{1}{(1 + \sqrt{p^2 + 4\pi m})^4}. \quad (29)$$

Although we do not yet have an analytical derivation for this approximation, it describes the scattering efficiencies quite well for most values of p, not only for the specular reflection but also for higher diffraction orders, except in the vicinity of $p = 2\sqrt{\pi m}$. To show the quality of the approximation (29), the reflectivity $R_m(p)$ versus $q_m(p) = \sqrt{p^2 + 4\pi m}$ is plotted in Fig. 7. The data from Fig. 6 were used, but data for $2 < m < 9$ are added to show that the trend (29) holds for large orders of scattering. In particular, for $p = 1$, this estimate is shown also in Fig. 5. This estimate will be easier to use in the planning of experiments than the full calculation.

D. Comparison of estimates

The simple estimate (8) describes well the experimental data [29,31] for the specular reflection. The fit (27) describes well the results of numerical simulations. The difference between these two functions can be seen in Fig. 6, by comparing the dashed line to the lower of the solid lines. The direct simulation predicts a reflectivity slightly higher than that observed in experiments. This difference was not expected; the direct simulation was supposed to fit the experimental data better than the rough estimate does. This motivated us to check our simulations with the independent analysis below.

IV. ANALYTICAL SOLUTION

The beam propagation method used in the preceding section automatically takes into account the discrete character of the absorbers. The results in the case of a set of periodic idealized absorbers were unexpected and require an independent confirmation. In this section we confirm these results with the analytical expansion that explicitly takes into account the periodicity of the ridges. Just as in the case of the numerical simulation, we ignore the structure of the ridges and assume them to be idealized thin edges.

A. Mathematical description

The periodicity of the mirror leads to the symmetry of the scattered wave; the translation for one period in the x direction should rotate the phase of the field by some angle. This

angle is determined by the incident wave. The symmetry of the solution allows the simplification of the solution and construction of the eigenfunction (see Refs. [37–40] and references therein). Such a discrete translational symmetry is referred to as the Bloch theorem or the Floquet theorem. However, for our scalar equation in the limit of small grazing angles, the formulas look simpler than the general expressions.

We again use the dimensionless variables as in the preceding section. The field should satisfy the same condition of quasiperiodicity,

$$E(X + 1, Y) = E(X, Y)\exp(-ip^2/2). \quad (30)$$

We search for the solution in the following form:

$$E(X, Y) = E_{ini}(X, Y) - \sum_m r_m e^{iq_m Y - (i/2)q_m^2 X}, \quad (31)$$

where $q_m = q_m(p)$ are defined by Eq. (23). In order to get an accurate estimate with only a few terms in the expansion, we also consider negative values of m. For $m < 0$, we may have imaginary wave numbers which correspond to exponentially decaying waves, similar to surface plasmons. The components with positive values of q_m are the various orders of scattering, and the square of modulus of the coefficient r_m has the sense of an intensity in the mth scattered wave. In particular, $|r_0|^2 = R$ is the coefficient of specular reflection.

Using the Green function (Kirchhoff integral) for the equation of Ginsburg-Landau, we get for the propagation from ridge number 0 to ridge number 1,

$$F(1, Y) = \frac{1}{\sqrt{2i\pi}} \int_0^\infty F(0, Y)e^{(i/2)(Y - Z)^2}dZ. \quad (32)$$

This gives the equation

$$e^{-ipY} - \sum_m r_m e^{iq_m Y} = \frac{1}{\sqrt{2i\pi}} \int_0^\infty e^{-ipX}e^{(i/2)(Y - Z)^2}dZ$$
$$- \frac{1}{\sqrt{2i\pi}} \int_0^\infty \sum_m r_m e^{(i/2)(Y - Z)^2}dZ.$$

Changing the order of summation and integration and collecting terms with coefficients r on the left-hand side of the equation, we obtain

$$\sum_m \left(e^{iq_m Y} - \frac{1}{\sqrt{2i\pi}} \int_0^\infty e^{(i/2)(Y - Z)^2}dZ \right) r_m$$
$$= e^{ipY} - \frac{1}{\sqrt{2i\pi}} \int_0^\infty e^{ipZ}e^{(i/2)(Y - Z)^2}dZ. \quad (33)$$

In order to simplify the deduction, we use the complementary error function [43],

$$\text{erfc}(z) = 1 - \text{erf}(z) = 1 - \frac{2}{\sqrt{\pi}} \int_0^z e^{-t^2}dt. \quad (34)$$
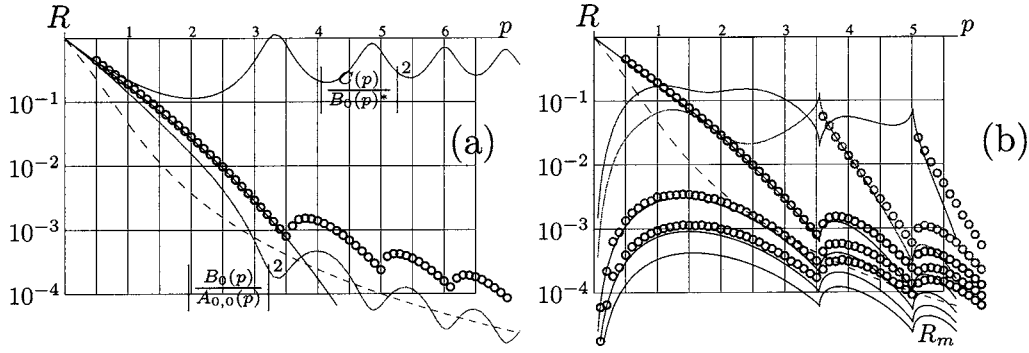
Then we rewrite Eq. (33) as follows:

FIG. 8. (a) The zeroth order approximation, $|r_0|^2$ by Eq. (47), lower oscillating line; $|r_0(p)|^2$ by the numerical solution described in the preceding section (circles) with its fit (solid line) by Eq. (27); the simple estimate by Eq. (8), dashed curve. The upper oscillating curve shows the upper estimate $|C(p)/B_0(p)|^2$. (b) Similar calculus with six waves taken into account; R_m are plotted with solid lines for $-3 \leq m \leq 2$. Circles correspond to the simulation, $-2 \leq m \leq 2$.

$$\sum_m e^{-g_m Y} \operatorname{erfc}\left(\frac{Y - ig_m}{1 + i}\right) r_m = e^{-ipY} \operatorname{erfc}\left(\frac{Y + p}{1 + i}\right), \quad (35)$$

where

$$g_m = \sqrt{-4\pi m - p^2} = -iq_m. \quad (36)$$

Formally, the complex reflectivity amplitudes r_m are determined as the solution of Eq. (35). For the estimates, we take only a finite number of components. Then, the substitution of the expansion (31) into Eq. (35) gives some residual. Its norm can be expressed as follows:

$$J = \int_0^\infty \left| \sum_m e^{-g_m Y} \operatorname{erfc}\left(\frac{Y - ig_m}{1 + i}\right) r_m - e^{-ipY} \operatorname{erfc}\left(\frac{Y + p}{1 + i}\right) \right|^2 dY. \quad (37)$$

We rewrite this residual in the following form:

$$J = r_m^* A_{m,n} r_n - r_m B_m^* - r_m^* B_m + C, \quad (38)$$

where we assume summation by the repeating subscripts,

$$A_{m,n} = A(g_m^*, g_n), \quad (39)$$

$$B_m = A(g_m^*, ip), \quad (40)$$

$$B_m^* = A(-ip, g_m), \quad (41)$$

$$C = A(-ip, ip), \quad (42)$$

$$A(u, v) = \int_0^\infty e^{-(u+v)t} \operatorname{erfc}\left(\frac{t + iu}{1 - i}\right) \operatorname{erfc}\left(\frac{t - iv}{1 + i}\right) dt. \quad (43)$$

The minimization of the residual J gives an equation for the array r of reflectivities which can be written in matrix form, i.e., $Ar = B$. Then, the solution can be written as follows:

$$r = A^{-1}B. \quad (44)$$

Let the subscripts m, n in Eqs. (37) and (38) run from m_1 to m_2. The parameters m_1 and m_2 determine the choice of scattered waves taken into account and specify the approximation for reflectivities $R_m = |r_m|^2$.

B. Upper and lower estimates

The simplest estimate corresponds to the single scattered component. Let $m_1 = m_2 = 0$,

$$A_{0,0} = \int_0^\infty \operatorname{erfc}\left(\frac{t - p}{1 - i}\right) \operatorname{erfc}\left(\frac{t - p}{1 + i}\right) dt, \quad (45)$$

$$B_0 = \int_0^\infty e^{-2ip} \operatorname{erfc}\left(\frac{t + p}{1 - i}\right) \operatorname{erfc}\left(\frac{t - p}{1 + i}\right) dt, \quad (46)$$

and we obtain the following estimates for the intensity of the specular reflection:

$$R_0 = |r_0(p)|^2 = \left| \frac{B_0}{A_{0,0}} \right|^2. \quad (47)$$

This function is shown in Fig. 8(a) as the lower solid line. This curve underestimates the reflectivity of the idealized ridged mirrors. At $p < 1$, it nearly coincides with the numerical solution of the preceding section. At large values of p, the corresponding estimate of the reflectivity $|r_0|^2$ oscillates around the estimate $R_z(p)$ by Eq. (8), shown by the dashed curve. (This dashed curve is the same as in Fig. 3 and Fig. 6.)

Similarly, we can estimate r_0 as

$$r_{0,\text{up}} = C(p)/B_0(p) \quad (48)$$

which gives the upper estimate for R_0; the function $|r_{0,\text{up}}|^2$ is shown in Fig. 8(a) with the upper solid curve.

At $p < 1$, the upper and lower estimates bracket the reflectivity obtained from the numerical solution in a narrow interval. For larger values of the normalized momentum p, we need to consider more harmonics in the expansion (31).

C. Orders of scattering

The agreement of the estimates based on the expansion (31) with the numerical solution can be improved by enlarging the interval $m_1 \leq m \leq m_2$. Here we consider the example while six harmonics were taken into account.

Figure 8(b) shows the behavior of reflectivities $R_m = |r_m(p)|^2$ evaluated with $m_1 = -2$, $m_2 = 3$ (solid lines). The circles correspond to lowest orders of scattering simulated in
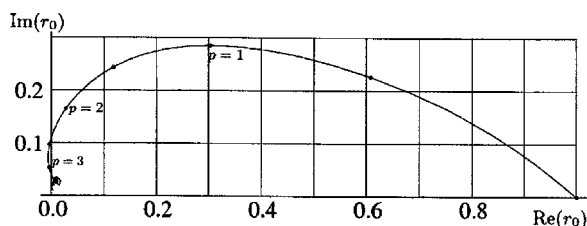
FIG. 9. Imaginary part of the amplitude r_0 of the specular reflection versus its real part.

the preceding section, R_m for $-2 \leqslant m \leqslant 2$ are shown. We see that it is sufficient to include only a few terms in the expansion (31) in order to estimate the efficiency of low orders of scattering.

The calculation of the specular reflectivity using six terms in the expansion ($m_1 = 3, m_2 = 2$) shows a very good agreement with the numerical simulations for values $p < 4$; the intensities of first and minus first orders are also reproduced quite well. If more terms are included in the expansion (31), a larger number of higher scattering orders can be accurately described.

D. Phase of the reflected wave

In Fig. 9 we plot the dependence of the imaginary part of the reflection amplitude r_0 versus its real part. Typically, the phase of the reflected wave is of the order of 1 radian. The phase information will be important for the creation of low-noise amplitude-phase holograms. A reflection-type amplitude hologram for atomic waves has recently been realized by Shimizu and Fujita [26]. A binary pattern was fabricated on a silicon surface that consisted of high-reflecting ridged surface areas and low-reflecting flat surface areas. We may expect the recent advances in the nanotechnology (see, for example, Refs. [41,42] and references therein) to lead to the next generation of efficient atom mirrors and amplitude-phase atomic holograms. In these holograms, the amplitude of the reflected wave can be adjusted with the distance L between ridges, and the phase can be adjusted with the height of the ridges. This height causes a phase shift

$$\phi = 2hk \sin(\theta), \tag{49}$$

where h is the relative displacement of the top of the ridges, $k = MV/\hbar$ is wave number, and θ is the grazing angle. The amplitude of the reflected wave can be adjusted with the distance L between ridges. However, this distance affects not only the amplitude of the scattered wave, but also its phase, causing an additional phase shift according to Fig. 9.

E. Limits of the approximation

We have analyzed the Fresnel scattering of a wave coming with a small grazing angle to the set of idealized ridges [Fig. 1(b)]. The analytical expansion of the scattered wave confirms the results of the beam propagation simulations described in the preceding section.

However, the coefficient of specular reflection of waves from idealized ridges still deviates from the simple estimate

R_z by Eq. (8) and therefore, from experimental data [29,31] [which agree with the estimate (8)]. This deviation should be attributed to some physical factors. We consider this deviation in the next section.

V. THE FINITE WIDTH OF THE RIDGES AND THE VAN DER WAALS POTENTIAL

If we compare the experimental data from Refs. [29,31] to the reflectivity calculated for a set of idealized ridges, then we see that the experimentally observed reflectivity is lower than the calculated one. However, the experimental data still obey a nearly exponential decay with parameter p, i.e., $R(p) \approx \exp(-ap)$, where a is almost constant. Comparing the exponential fit $\exp(-\sqrt{8}p) \approx \exp(-2.8p)$ and the fit (27) we guess that some effect drops the reflectivity by an additional factor of order $\exp(-1.1p)$. In this section we attribute this drop to the van der Waals interaction. This interaction makes the main differences between the typical experimental situation and our model [Fig. 1(b)].

For the scattering at the periodical surface, the resonant contributions of various ridges are important. The van der Waals interaction in the vicinity of the ridges provides some effective refraction index which destroys the phase synchronism in the scattered waves. We analyze in the following the role of this effect and suggest the corresponding correction to the reflection coefficient.

A. Reduction of reflectivity

We assume that the van der Waals interaction of atoms with a surface can be approximated with the potential $U(x,y) \approx -C_n/y^n$, where y is the distance between the atom and the surface; $n = 3$ for the unretarded potential and $n = 4$ for the retarded case. Approximate values for the constants C_4 are given in Table I.

For the atomic matter waves, the potential appears as a variation of the index of refraction. When the ridges are narrow, we can estimate the corresponding correction to the phase in the Raman-Natch approximation. Consider the trajectory $y(x)$. We then estimate the additional phase shift $\Phi(y)$ caused by the van der Waals potential to be

$$\Phi(y) \approx \int U(x,y(x)) \frac{\mathrm{d}x}{\hbar V} = \int \frac{C_n}{y^n} \frac{\mathrm{d}x}{\hbar V} \approx \frac{C_n}{y^n \hbar V} D, \tag{50}$$

where D is the effective length that the atom passes in vicinity of the ridge. An exact calculation of this length D is complicated. In order to obtain a simple estimate, we set $D \approx \ell + 2s$, where s is some typical distance between a marginal trajectory (which still contributes to the specular reflection) and the edge of the ridge. If the phase shift is getting large, i.e., $\Phi \approx 1$ radian, then we can assume that this part of the wave does not contribute much to the Fresnel integral. The marginal distance s where this condition is fulfilled can be estimated from the equation

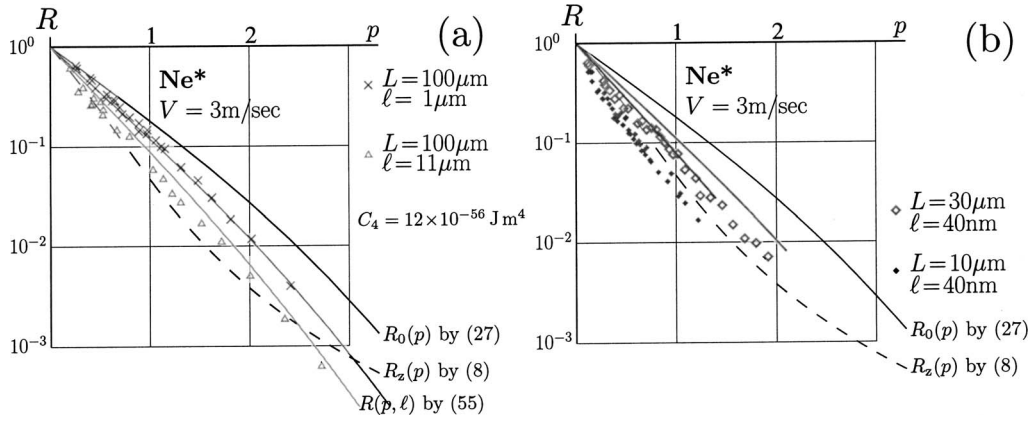$$s = \left(\frac{(\ell + 2s)C_n}{\hbar V} \right)^{1/n}. \tag{51}$$

FIG. 10. Estimate (55) and data for Ne*.

On the other hand, the main contribution to the Kirchhoff integral comes from the vicinity of ridges. The size of this region can be estimated to be

$$s_0 = 1/(k\theta). \tag{52}$$

This region would generate a reflected wave of intensity $R_0(p)$; we can use the fit (27) for the idealized ridges. However, the (s/s_0)th part of this wave is out of phase due to the potential. Therefore, we may assume that the intensity of the reflected wave will be reduced by the factor $1 - s/s_0$, i.e.,

$$R(p,\ell) \approx \left(1 - \frac{s}{s_0}\right)R_0(p). \tag{53}$$

This expression can only be applied when s is much smaller than s_0. To get a self-consistent estimate we should replace the first parentheses on the right-hand side of Eq. (53) with some smooth function of s/s_0, which has the same asymptotic behavior at small values of s, but remains positive at large values. In order to get a simple estimate, we replace the factor $[1 - (s/s_0)]$ by the appropriate exponential and suggest the following estimate:

$$R(p,\ell) = \exp\left(-\frac{s}{s_0}\right)R_0(p). \tag{54}$$

This leads to

$$R(p,\ell) = \exp\left(-\sqrt{\frac{mV}{\hbar L}}sp\right)R_0(p), \tag{55}$$

where $s = s(\ell)$ is defined by Eq. (51). The factor $\sqrt{(mV/\hbar L)}s$ is of order of unity for the cases shown in Table I, and almost proportional to $(\ell C_n)^{1/n}$. However, it is not a constant, but it is a slow function of p and its values are close to the coefficient 1.1 mentioned in the beginning of the section. Typically, ℓ is larger than the resulting s [see Eq. (51)]; then a variation of ℓ, C_3 or C_4 should not have a strong effect on the reflectivity.

B. Comparison of estimate (55) with experiments

There are two sets of data available where ℓ is the only parameter to vary. We compare the experimental data to the

correction (55), assuming $n = 4$, in Fig. 10. The crosses and triangles represent the experimental data for $\ell = 1$ μm and $\ell = 11$ μm, and two thin curves show the estimates by Eq. (55). The thick solid line represents the fit (27); the dashed line represents the estimate R_z by Eq. (8). The corrected estimate (55) is much closer to the experimental data than any of the estimates (8) and (27).

Note that the van der Waals constant C_4 is the only empirical parameter in this description, and values of this parameter are taken from the literature. The s value is calculated from Eq. (51); the straightforward iterative procedure converges quickly. In most cases, the estimate does not become much worse if we make only two or even one iteration and replace s by $(\ell C_4/\hbar V)^{1/4}$ on the right-hand side of Eq. (51). Therefore we may claim that our estimate is expressed in terms of elementary functions.

For $L = 100$ μm, the estimate (55) not only shows the limit of the approximation of the idealized ridges, but also gives the correction which shows very good agreement with experiments [Fig. 10(a)]. For the samples with $\ell = 40$ nm, our correction (55) slightly overestimates the reflectivity observed in experiments [Fig. 10(b)]. However, our estimate still shows the correct order of magnitude and still explains why the estimate R_z by Eq. (8) happens to be so close to the experimental data.

In the case of He*, we plot the expected reflectivities according to the estimate Eq. (55) in Fig. 11. As we already mentioned, the correction does not depend much on the velocity V of atoms; in the logarithmic scale, these lines are almost straight and almost coincide. Again, we see very good agreement between the estimate Eq. (55) and the experimental data. The finite width of the ridges partially compensates the periodic character of the absorbing ridges. This explains the good agreement of the simple estimate $R_z(p)$ by (8) with experimental data.

VI. CONCLUSIONS

The reflection of cold atoms from ridged, gratinglike surfaces was analyzed using a formalism borrowed from wave optics. The case of small grazing angle is considered.

(1) For the specular reflection of waves, the ridged surface can be interpreted as an equivalent continuously absorbing
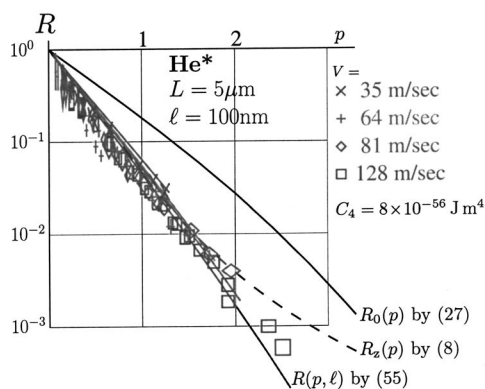
FIG. 11. Estimate (55) and data for He*.

medium. This approximation gives the estimate $R_z(p)$ by Eq. (8) for the reflectivity. This estimate depends only on the dimensionless momentum $p = \sqrt{kL}\theta$, and reveals the important scaling law for the efficiency of the ridged mirrors. No assumptions about the nature of the waves is used at this step. Such simple estimate shows good agreement with experimental data [29,31] on the reflection of cold excited Ne and He atoms from ridged Si surfaces in a wide range of values of physical parameters (Table I).

(2) A more detailed description is obtained from the consideration of the diffraction of the wave by a set of idealized edges. The reflectivity and intensities of several diffraction orders have been determined with numerical simulations and confirmed with an independent analytical expansion. The reflectivity can be approximated with an empirical fit (27). This fit describes well the simulations but slightly overestimates the reflectivity of atomic mirrors. The correction (55) of the reflection coefficient due to van der Waals interaction shows the limits of the thin ridges approximation. In most cases, such a correction shows very good quantitative agreement with experiments. The deviation of the experimental data from estimate (55) is of order of experimental errors marked in Fig. 11.

(3) The phase of the reflected wave and the efficiency of lower orders of scattering are estimated on the base of the model of thin absorbing ridges. These estimates can be useful for the construction of advanced phase-amplitude atom holograms. The efficiency of scattering into the minus first order of diffraction is larger than that of the specular reflection (Fig. 5). This indicates the possibility of measurement of this scattering order with cold atoms.

(4) The possible improvement of estimate (55) may include a more sophisticated fit (for example, two-parametric) for the van der Waals interaction, as well as a more accurate evaluation of integral (50). For the specular reflection, such improvement may lead to an adjustment of a few percent of transversal velocity v, at which the given reflectivity takes place, rather than revealing a physical phenomenon. However, such an analysis may be useful for the accurate estimate of amplitude and phase of various orders of scattering. Also, such a sophisticated analysis can be useful for the prediction of properties of ridged mirrors with nontrivial profile of the edges of the ridges.

(5) The specular reflection of waves from ridged surfaces is not sensitive to the nature of the waves; only the wave vector is important. The ridged mirrors should reflect the ground-state atoms as well as the excited atoms. It is interesting to compare our estimates to the experimental data with other kinds of waves, ground-state atoms, photons, phonons and/or neutrons. The deviation of the coefficient of the specular reflection from the estimate (55) can be used as a short-distance probe of the van der Waals interaction, as well as a criterion of perfection of ridged surfaces. We expect this criterion to work for various kinds of waves. The estimates (8), (27), and (55) should be useful in the design of ridged mirrors for various applications including atom optics. For atoms, these estimates show that the reduction of distance L between ridges and their width ℓ improves the reflectivity and/or extends the range of working angle.

[1] H. Katori and T. Akatsuka, Jpn. J. Appl. Phys., Part 1 **43**, 358 (2004).

[2] R. Folman, P. Kruger, J. Schmiedmayer, J. Denschlag, and C. Henkel, Adv. At., Mol., Opt. Phys. **48**, 263 (2002).

[3] V. Balykin, V. Klimov, and V. Letokhov, Opt. Photonics News **16**, 44 (2005).

[4] V. I. Balykin, V. S. Letokhov, Y. B. Ovchinnikov, and A. I. Sidorov, Phys. Rev. Lett. **60**, 2137 (1988).

[5] M. Kasevich, D. Weiss, and S. Chu, Opt. Lett. **15**, 607 (1990).

[6] H. Oberst, S. Kasashima, V. I. Balykin, and F. Shimizu, Phys. Rev. A **68**, 013606 (2003).

[7] C. V. Saba, P. A. Barton, M. G. Boshier, I. G. Hughes, P. Rosenbusch, S. E. Sauer, and E. A. Hinds, Phys. Rev. Lett. **82**, 468 (1999).

[8] D. C. Lau, R. J. McLean, A. I. Sidorov, D. S. Gough, J. Koperski, W. J. Rowlands, B. A. Sexton, G. I. Opat, and P. Hannaford, J. Opt. B: Quantum Semiclassical Opt. **1**, 371 (1999).

[9] M. Drndić *et al.*, Phys. Rev. A **60**, 4012 (1999).

[10] B. Poelsema and G. Comsa, *Scattering of Thermal Energy Atoms from Disordered Surfaces*, Springer Tracts in Modern Physics, Vol. 115 (Springer-Verlag, Berlin, Heidelberg, 1989).

[11] *Helium Atom Scattering from Surfaces*, edited by E. Hulpke, Springer Series in Surface Sciences, Vol. 27 (Springer-Verlag, Berlin, Heidelberg, 1992).

[12] A. Anderson, S. Haroche, E. A. Hinds, W. Jhe, D. Meschede, and L. Moi, Phys. Rev. A **34**, 3513 (1986).

[13] F. Shimizu, Phys. Rev. Lett. **86**, 987 (2001).

[14] A. Mody, M. Haggerty, J. M. Doyle, and E. J. Heller, Phys. Rev. B **64**, 085418 (2001).

[15] E. Krotscheck, V. Apaja, and A. Rimnac, Physica B **329–333**, 260 (2003).

[16] D. P. Clougherty and W. Kohn, Phys. Rev. B **46**, 4921 (1992).

[17] C. Carraro and M. W. Cole, Prog. Surf. Sci. **57**, 61 (1998).

[18] R. B. Doak and A. V. G. Chizmeshya, Europhys. Lett. **51**, 381 (2000).

[19] H. Friedrich, G. Jacoby, and C. G. Meister, Phys. Rev. A **65**, 032902 (2002).

[20] A. Jurisch and H. Friedrich, Phys. Rev. A **70**, 032711 (2004).

[21] H. Friedrich, Phys. World **17** (8) pp. 20–21 (August, 2004).

[22] V. U. Nayak, D. O. Edwards, and N. Masuhara, Phys. Rev. Lett. **50**, 990 (1983).

[23] I. A. Yu, J. M. Doyle, J. C. Sandberg, C. L. Cesar, D. Kleppner, and T. J. Greytak Phys. Rev. Lett. **71**, 1589 (1993).

[24] J. J. Berkhout, O. J. Luiten, I. D. Setija, T. W. Hijmans, T. Mizusaki, and J. T. M. Walraven, Phys. Rev. Lett. **63**, 1689 (1989).

[25] J. M. Doyle, J. C. Sandberg, I. A. Yu, C. L. Cesar, D. Kleppner, and T. J. Greytak, Phys. Rev. Lett. **67**, 603 (1991).

[26] F. Shimizu and J. I. Fujita, Phys. Rev. Lett. **88**, 123201 (2002).

[27] V. Druzhinina and M. DeKieviet, Phys. Rev. Lett. **91**, 193202 (2003).

[28] T. A. Pasquini, Y. Shin, C. Sanner, M. Saba, A. Schirotzek, D. E. Pritchard, and W. Ketterle, Phys. Rev. Lett. **93**, 223201 (2004).

[29] F. Shimizu and J. Fujita, J. Phys. Soc. Jpn. **71**, 5 (2002).

[30] H. Oberst, M. Morinaga, F. Shimizu, and K. Shimizu, Appl. Phys. B: Lasers Opt. **76**, 801 (2003).

[31] H. Oberst, D. Kouznetsov, K. Shimizu, J. I. Fujita, and F. Shimizu, Phys. Rev. Lett. **94**, 013203 (2005).

[32] D. Kouznetsov and H. Oberst, http://www.ils.uec.ac.jp/~dima/zeno.pdf (Opt. Rev., to be published).

[33] D. Yu. Kuznetsov, Transformation of spatial structure of monochromatic radiation in nonlinear media, in *Nonlinear and Quantum Optical Phenomena in Equilibrium Media*, edited by V. A. Shcheglov, pp. 1–119 (Nova Science Publishers, Inc., New York, 1993).

[34] D. Kouznetsov, J. V. Moloney, and E. M. Wright, J. Opt. Soc. Am. B **12**, 743 (2001).

[35] D. Kouznetsov and J. V. Moloney, J. Opt. Soc. Am. B **19**, 1259 (2002).

[36] J. V. Moloney and A. C. Newell, *Nonlinear Optics* (WestView Press, 2004).

[37] P. Sheng, R. S. Stepleman, and P. N. Sanda, Phys. Rev. B **26**, 2907 (1982).

[38] J. R. Manson, "Theoretical aspects of atom-surface scattering," in *Helium Atom Scattering from Surfaces*, edited by E. Hulpke (Springer-Verlag, Berlin, Heidelberg, 1992) pp. 173–205.

[39] P. C. Logofatu, S. A. Coulombe, B. K. Minhas, and J. R. McNeil, J. Opt. Soc. Am. A **16**, 1108 (1999).

[40] H. Jia and K. Yasumoto, Int. J. Infrared Millim. Waves **25**, 1591 (2004).

[41] S. C. Lee and S. R. J. Brueck, J. Vac. Sci. Technol. B **22**, 1949 (2004).

[42] S. C. Lee, L. R. Dawson, B. Pattada, S. R. J. Brueck, Y.-B. Jiang, and H. F. Xu, Appl. Phys. Lett. **85**, 4181 (2004).

[43] M. Abramovitz and I. A. Stegun, *Handbook of Mathematical Functions* (National Bureau of Standards, Washington, DC, 1964).